AIP | Physics of Fluids

Inertia dominated drop collisions. II. An analytical solution of the Navier–Stokes equations for a spreading viscous film

Ilia V. Roisman

Citation: Phys. Fluids **21**, 052104 (2009); doi: 10.1063/1.3129283
View online: http://dx.doi.org/10.1063/1.3129283
View Table of Contents: http://pof.aip.org/resource/1/PHFLE6/v21/i5
Published by the AIP Publishing LLC.

Additional information on Phys. Fluids

Journal Homepage: http://pof.aip.org/
Journal Information: http://pof.aip.org/about/about_the_journal
Top downloads: http://pof.aip.org/features/most_downloaded
Information for Authors: http://pof.aip.org/authors

Downloaded 04 Oct 2013 to 141.161.91.14. This article is copyrighted as indicated in the abstract. Reuse of AIP content is subject to the terms at: http://pof.aip.org/about/rights_and_permissions

Inertia dominated drop collisions. II. An analytical solution of the Navier–Stokes equations for a spreading viscous film

Ilia V. Roisman
Chair of Fluid Mechanics and Aerodynamics, Technische Universität Darmstadt, Petersenstr. 30, 64287 Darmstadt, Germany

(Received 3 February 2009; accepted 7 April 2009; published online 11 May 2009)

This study is devoted to a theoretical description of an unsteady laminar viscous flow in a spreading film of a Newtonian fluid. Such flow is generated by normal drop impact onto a dry substrate with high Weber and Reynolds numbers. An analytical self-similar solution for the viscous flow in the spreading drop is obtained which satisfies the full Navier–Stokes equations. The characteristic thickness of a boundary layer developed near the wall uniformly increases as a square root of time. An expression for the thickness of the boundary layer is used for the estimation of the residual film thickness formed by normal drop impact and the maximum spreading diameter. The theoretical predictions agree well with the existing experimental data. A possible explanation of the mechanism of formation of an uprising liquid sheet leading to splash is also proposed. © *2009 American Institute of Physics*. [DOI: 10.1063/1.3129283]

I. INTRODUCTION

Drop impacting onto a dry smooth substrate creates a radially expanding film flow. If the impact parameters, Reynolds and Weber numbers, are high enough this film is relatively thin and is bounded by a rim formed by capillary forces. This phenomenon is similar to the formation of a rim bounding a free liquid sheet.[1,2] The flow in the lamella and the propagation of the rim determine the evolution of the drop spreading diameter.[3] At some instant the drop spreading diameter reaches the maximum and then, if the substrate is partially or nonwettable, recedes.

The maximum spreading diameter is one of the major criteria affecting the quality of ink-jet printing. Prediction of the lamella thickness is required for better design and optimization of the technology for spray encapsulation of solid particles in a fluidized bed,[4] for the modeling of spray coating, or for icing of plane wings. High shear stresses in the lamella are beneficial for better spray cleaning. On the other hand these stresses can lead to an undesirable substrate erosion, for example, in the agricultural applications.

A most recent comprehensive review on drop impact modeling can be found in Ref. 5. Most of the existing models estimate the typical thickness of the lamella as a function of the impact parameters: contact angle θ, impact Reynolds number $\mathrm{Re}=\rho D_0 U_0/\mu$, and Weber number $\mathrm{We}=\rho D_0 U_0^2/\sigma$, where D_0 and U_0 are the initial drop diameter and impact velocity and ρ, μ, and σ are the liquid density, viscosity, and surface tension, respectively.

A. Maximum spreading diameter

In some asymptotic cases a scaling analysis can be applied to the description of drop spreading. In Fig. 1 the scaling[6] for the dimensionless maximum spreading diameter (scaled by the initial drop diameter D_0), $D_{\max}\mathrm{Re}^{-1/5}$, of a drop impacting onto a dry superhydrophobic substrate is shown as a function of the parameter $P=\mathrm{WeRe}^{-4/5}$. In this figure two asymptotic regimes are combined. For the impact of a low-viscosity liquids ($P<1$) the maximum drop diameter is determined exclusively by the capillary number and can be scaled as $D_{\max}\sim\mathrm{We}^{1/4}$. This regime corresponds to curve S1 in Fig. 1. In the viscous regime ($P>1$), represented in Fig. 1 by curve S2, the maximum drop diameter is determined mainly by the impact Reynolds number, $D_{\max}\sim\mathrm{Re}^{1/5}$.

Another scaling relation for the maximum spreading diameter was proposed in Ref. 9. The dimensionless maximum spreading diameter can be represented as a function of the impact parameters in the form $K=\mathrm{Re}^{1/2}\mathrm{We}^{1/4}$. This scaling can allow to successfully predict the maximum spreading diameter in a wide range of the impact parameters (see Fig. 2). As shown in Fig. 3 a similar empirical scaling relation $D_{\max}=0.61K^{0.332}$, proposed in Ref. 10, also excellently agrees with the experimental data.

Since details of the flow in the deforming drop are not known, an energy balance approach is often used for the evaluation of the geometry of the spreading drop: its average height and maximum diameter.[7,11–13] In the theoretical studies on drop impact onto a dry substrate[3] and binary drop collision[14] the energy balance equation is used for the estimation of the lamella thickness and the initial velocity distribution in the spreading velocity. The most recent and probably the most refined model of such type[15] predicts the dimensionless maximum spreading diameter $D_{\max}$ of a drop impacted onto a dry substrate as a root of the dimensionless cubic equation

$$(\mathrm{We}+12)D_{\max}=8+D_{\max}^3[3(1-\cos\theta)+4\mathrm{WeRe}^{-1/2}]. \quad (1)$$

This model predicts very well the value of the maximum spreading diameter in a rather wide range of impact parameters. In Fig. 4 the predictions[15] calculated using Eq. (1) are compared with the experimental data for the maximum spreading diameter found in the literature.[3,7,8]

The theory for drop spreading and receding[3] can also be easily applied to the estimation of the maximum spreading

 © 2009 American Institute of Physics

Downloaded 04 Oct 2013 to 141.161.91.14. This article is copyrighted as indicated in the abstract. Reuse of AIP content is subject to the terms at: http://pof.aip.org/about/rights_and_permissions

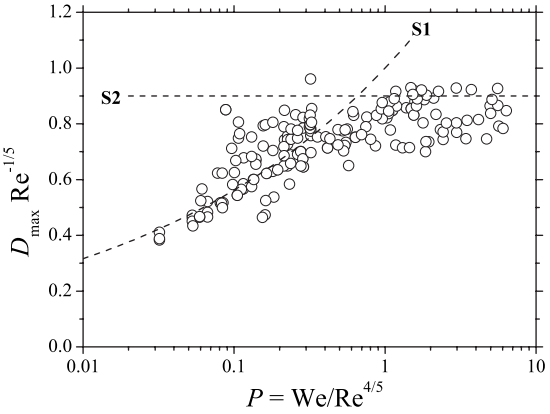

FIG. 1. Scaled maximum spreading diameter of a drop impacting onto a dry substrate as a function of the scaling parameter P proposed in Ref. 6. The experimental data are from Refs. 3 and 7–9. The dashed lines correspond to the experimental data (Ref. 6) for superhydrophobic surfaces.

diameter. In this study the average dimensionless height h_1 of the drop at the dimensionless time $t=1$ is estimated from the integral momentum balance equation

$$3We + 5(1 - \cos\,\theta)Re h_1 = 10ReWe h_1^3, \tag{2}$$

where θ is the average contact angle during spreading, which can be roughly estimated as $\theta \approx 130°$ if the Weber and Reynolds numbers are high.[16] The value of the drop diameter at this time instant is then estimated from the mass balance of the drop,

$$D_1 = \sqrt{\frac{2}{3h_1}}. \tag{3}$$

It can be shown that the value of the diameter D_1 can be also a good scale for the maximum spreading diameter. In Fig. 5 the experimental data for the maximum spreading diameter show almost linear dependence on D_1 estimated using Eqs. (2) and (3).

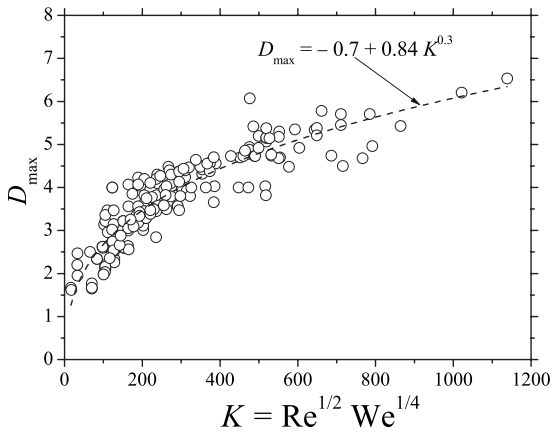

FIG. 2. Dimensionless maximum spreading diameter as a function of the scaling parameter $K=Re^{1/2}We^{1/4}$ proposed in Ref. 9. The experimental data are from Refs. 3 and 7–9.

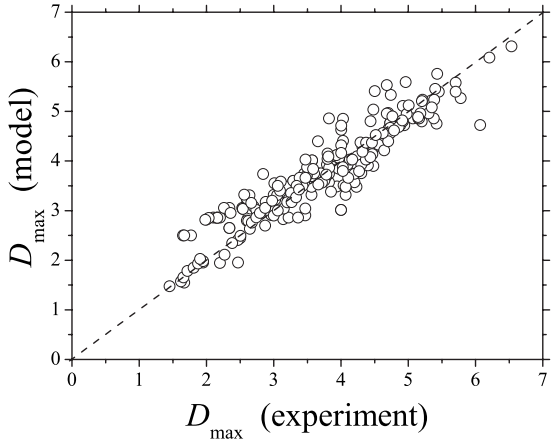

FIG. 3. Single drop impact onto a dry substrate. Comparison of the empirical correlation (Ref. 10) for the dimensionless maximum spreading diameter expressed as $D_{max}=0.61K^{0.332}$ with the experimental data from Refs. 3 and 7–10.

B. Recent developments

In an experimental study[4] the thickness of the lamella generated by an axisymmetric drop impact onto a spherical target is measured for various impact parameters and target diameters. It was shown that the evolution of the height of the drop at the symmetry axis almost does not depend on the impact Reynolds and Weber numbers. It depends mainly on the local curvature of the target.

During the first phase of drop deformation the height of the drop reduces linearly in time with almost constant velocity. Then, at the time instant $\sim 0.5D_0/U_0$ the thickness starts to follow the inverse square dependence of time, predicted by the remote asymptotic solution.[17] Finally, when the film thickness becomes comparable to the thickness of a viscous boundary layer, the flow in the film is governed by inertia and viscosity which eventually damps the velocity. The residual film thickness depends therefore on the Reynolds number and on the dimensionless diameter of the target particle.

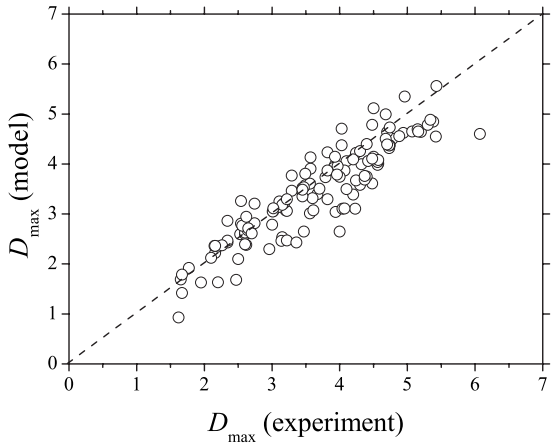

FIG. 4. Single drop impact onto a dry substrate. Comparison of the theoretical predictions (Ref. 1) for the dimensionless maximum spreading diameter expressed in Eq. (1) with the experimental data (Refs. 3, 7, and 8).

Downloaded 04 Oct 2013 to 141.161.91.14. This article is copyrighted as indicated in the abstract. Reuse of AIP content is subject to the terms at: http://pof.aip.org/about/rights_and_permissions

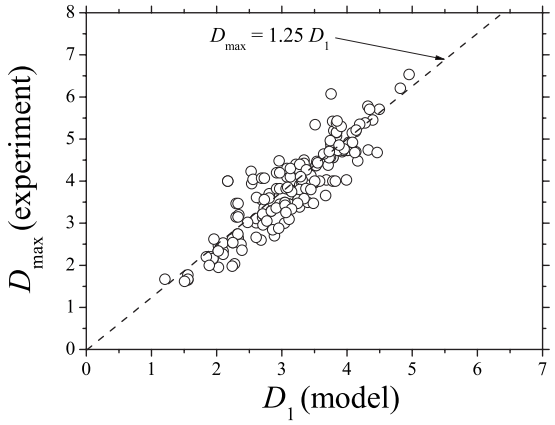

FIG. 5. Single drop impact onto a dry substrate. Dimensionless maximum spreading diameter as a function of the theoretically predicted initial drop diameter D_1 determined in Eqs. (2) and (3). The experimental data are from Refs. 3 and 7–9.

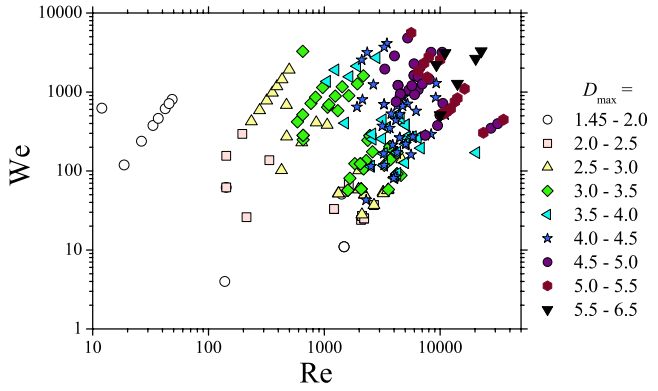

FIG. 6. (Color online) Impact parameters of the experiments (Refs. 3 and 7–10) used in Figs. 1–5 for validation of the existing models.

In a recent theoretical study[18] a universal flow in the lamella, which does not depend on the impact parameters, is used to describe the evolution of the diameter of the drop produced by a double-symmetric binary droplet collision or normal impact onto a dry substrate if the impact Weber and Reynolds numbers are high. This result contradicts all the previous drop impact models which relate the parameters of drop spreading to the impact Reynolds and Weber numbers.

Moreover, as was recently mentioned[19] and then demonstrated in Ref. 18, the energy balance approach in its "conventional" form is not applicable to the description of drop impact and spreading since the edge effects associated with the rim formation are not always properly accounted for. Therefore, principally new approaches have to be applied to the modeling of the phenomena associated with drop impact.

The numerical predictions[18] show that the dimensionless flow in the central, inner region in the lamella (scaled by the impact velocity U_0) is described well by the remote asymptotic solution[20]

$$v_r = \frac{r}{t+\tau}, \quad v_z = -\frac{2z}{t+\tau} \tag{4}$$

and the thickness of the lamella can be roughly approximated by the Gaussian function of r,

$$h_L = \frac{\eta}{(t+\tau)^2}\exp\left[-\frac{6\eta r^2}{(t+\tau)^2}\right], \tag{5}$$

where τ is an inverse of the initial gradient of the radial velocity and η is a constant related to the initial film thickness. The values $\eta \approx 0.39$ and $\tau \approx 0.25$ are estimated from the experimental data[4] and numerical simulations.[13,16,18,21] The expression for the shape of the lamella [Eq. (5)] is valid for the relatively large times after impact far from the rim region.

C. Summary on the modeling of drop spreading

The models described above predict well the maximum spreading diameter in a rather wide range of impact parameters, shown in Fig. 6. Some of these models, based on the energy balance or on the approximation of the drop shape by a disk, include internal contradictions.[18] Nevertheless, these results have practical importance even as empirical correlations.

It should be also noted that the existing scaling relations[6,9] for drop/wall interaction are not applicable to the prediction of binary drop collisions despite the fact that the geometry of these two phenomena are very similar. The only difference between them is in the development of the near-wall boundary layer developed immediately after drop impact onto a dry substrate. During binary drop collision this viscous layer does not appear since the inviscid flow (4) satisfies boundary conditions at the symmetry plane. As a result the maximum spreading diameter in the case of binary drop collision is much larger than analogous drop impact onto a rigid substrate.

An actual controversy is, however, that the existing theoretical approaches to the problem are based on very different main assumptions. These assumptions reflect our understanding of the major factors influencing the flow in the spreading drop. Numerous existing scaling relations have often very different forms. Therefore, despite the fact that these models are validated by a large number of experimental data on the maximum drop diameter, it is not clear which assumptions are relevant and whether the models describe correctly the hydrodynamics of drop spreading.

D. Subject of the present study

The evolution of the drop diameter already at the relatively early stages of drop spreading (at dimensionless times $t > 0.1$) depends significantly on the impact Reynolds number.[22] This effect is caused by the development of a viscous boundary layer near the wall and by formation of the rim as the result of the action of capillary forces applied to the edge of the lamella.[3]

The evolution of the thickness of the boundary layer can be roughly estimated as $h_{BL} \sim \sqrt{t/\mathrm{Re}}$ using the analogy with the Stokes first problem. However, it is not yet clear whether

Downloaded 04 Oct 2013 to 141.161.91.14. This article is copyrighted as indicated in the abstract. Reuse of AIP content is subject to the terms at: http://pof.aip.org/about/rights_and_permissions

this result can be directly applied to the axisymmetric remote asymptotic flow (4). In particular, it is important to determine how the inertial effects, velocity gradient in the radial direction, pressure gradient in the axial direction, and axial velocity component influence the development of the boundary layer.

The present paper is devoted to the description of an axisymmetric instationary viscous flow in a spreading film of Newtonian liquid generated by normal drop impact onto a rigid, planar, dry substrate. An analytical self-similar solution for the velocity distribution in the viscous flow is obtained which satisfies the full Navier–Stokes equations.

The rate of the growth of the boundary layer thickness is then used for the development of a new scaling model for the maximum spreading diameter of the impacting drop. The theory allows to accurately estimate also the thickness of the residual film on the substrate formed by drop impact.

II. VISCOUS FLOW IN A RADIALLY SPREADING LIQUID FILM

A. Self-similar analytical solution

The remote asymptotic solution[17] for the inertia dominated inviscid flow on a wall valid for the long times after the flow initiation is assumed in the following approximate form:

$$v_{r0} = \frac{r}{t}, \quad v_{z0} = -\frac{2z}{t} + Z(t), \quad Z(0) = 0 \tag{6}$$

since the constant τ in Eq. (4) is relatively small. It can be shown that for any arbitrary function $Z(t)$ the flow satisfies the continuity and the full Navier–Stokes equations even if the viscosity effects in the flow are significant. The pressure gradient and the gradients of the deviatoric stresses in the radial direction vanish. However, this flow does not satisfy the no-slip condition at the wall, $z=0$.

Let us find a viscous flow $\{v_r, v_z\}$ which satisfies the wall boundary conditions at $z=0$ and approaches the remote approximate solution (6) at $\{z \to \infty \forall t > 0\}$ and at $\{t \to 0 \forall z > 0\}$. The stream function of the flow is assumed in the form $\psi(r,z,t) = r^2 f(z,t)$, where $f(z,t)$ is still an unknown function of z and t. The components of the velocity field which satisfies the continuity equation can be now determined as

$$v_r = \frac{\psi_{,z}}{r} = r f_{,z}, \quad v_z = -\frac{\psi_{,r}}{r} = -2f, \tag{7}$$

where the subscript $(,z)$ denotes partial differentiation with respect to z.

Function f must satisfy the following boundary conditions:

$$f = 0, \quad f_{,z} = 0 \quad \text{at } z = 0, \tag{8}$$

$$f_{,z} = \frac{1}{t} \quad \text{at } z \to \infty, \tag{9}$$

and will be found from the solution of the momentum balance equation in the radial direction. From the momentum balance equation in the axial z direction it can be easily shown that the pressure corresponding to the flow field in the assumed form (7) is a function of the axial coordinate z only and does not depend on the radius r.

The momentum balance equation in the radial direction for an axisymmetric flow in the absence of the pressure gradient and body forces reduces to the following equation:

$$\frac{\partial v_r}{\partial t} + v_r \frac{\partial v_r}{\partial r} + v_z \frac{\partial v_r}{\partial z} = \nu \left\{ \frac{\partial}{\partial r}\left[\frac{1}{r} \frac{\partial (r v_r)}{\partial r} \right] + \frac{\partial^2 v_z}{\partial z^2} \right\}, \tag{10}$$

where ν is the kinematic viscosity. Substitution of the velocity field (7) in Eq. (10) yields the following partial differential equation for function $f(z,t)$:

$$f_{,z}^2 + f_{,zt} - 2 f f_{,zz} - \nu f_{,zzz} = 0. \tag{11}$$

Let us introduce the usual self-similar variable

$$\xi = \frac{z}{\sqrt{\nu t}}, \tag{12}$$

based on the expression for the viscous length $\sqrt{\nu t}$. The form for the function $f(z,t)$ can be found rewriting the boundary condition (9) as $f_{,\xi} = \sqrt{\nu / t}$ at $\xi \to \infty$. A self-similar solution for the flow in the boundary layer can be therefore obtained if the function f is represented in the form

$$f(z,t) = \frac{\sqrt{\nu}}{\sqrt{t}} g(\xi), \tag{13}$$

where $g(\xi)$ is the scaled stream function. Substituting Eq. (13) in Eq. (11) yields

$$g''' + 2 g g'' + \tfrac{1}{2} \xi g'' + g' - g'^2 = 0, \tag{14}$$

where the prime denotes the derivative in respect to the self-similar variable ξ. The ordinary differential equation (14) for the scaled stream function g can be solved numerically subject to the boundary conditions

$$g = 0, \quad g' = 0 \quad \text{at } \xi = 0, \tag{15}$$

$$g' = 1 \quad \text{at } \xi \to \infty, \tag{16}$$

Equations (14)–(16) form a nonlinear boundary value problem. We have solved numerically the ordinary differential equation (14) subject to the initial conditions (15) for various values of the initial second derivative $g''(0)$ in order to find a solution which satisfies the boundary condition (16) at infinity. Finally two solutions of Eq. (14) are determined corresponding to the adjusted initial conditions $g''(0) = -0.618\,925$ and $g''(0) = 1.0354$.

The solution satisfying $g''(0) = -0.618\,925$ is associated with the separated boundary layer with the negative wall shear stress. This solution predicts the flow in the positive z direction at $\xi < 4$. This nonphysical solution is not considered in the present study.

The solution corresponding to $g''(0) = 1.0354$ is shown in Fig. 7. The characteristic boundary layer thickness corresponding to $g'(\xi) = 0.99$ is uniform (does not depend on the radial coordinate r) and can be estimated from the numerical solution as

$$\delta_{0.99} = 1.88 \sqrt{\nu t}. \tag{17}$$

Downloaded 04 Oct 2013 to 141.161.91.14. This article is copyrighted as indicated in the abstract. Reuse of AIP content is subject to the terms at: http://pof.aip.org/about/rights_and_permissions

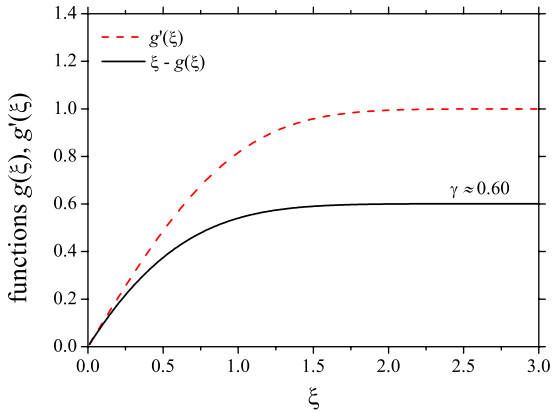

FIG. 7. (Color online) Scaling functions $g(\xi)$ and $g'(\xi)$.

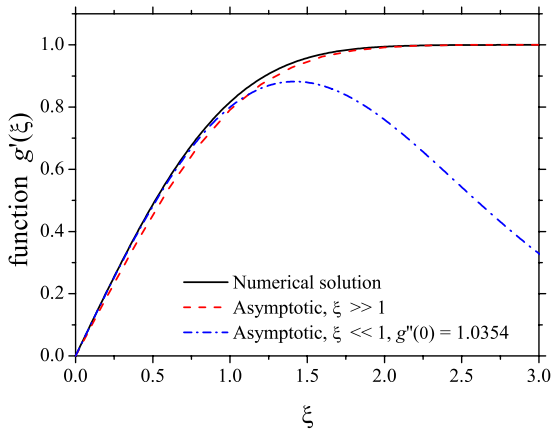

FIG. 8. (Color online) Approximate solutions for the function $g'(\xi)$.

This value is much smaller than the corresponding thickness of the boundary layer in the two-dimensional first Stokes problem. The reason is the presence of the negative component of the velocity in the normal-to-the-wall direction and in the positive velocity gradient in the radial direction.

The expanding viscous boundary layer generates an additional liquid flow also in the vertical direction. As shown in Fig. 7 the value of function $\xi - g(\xi)$ asymptotically approaches some constant $\gamma \neq 0$ if $\xi \to \infty$. The value of the constant $\gamma = 0.60$ is determined from the numerical solution of Eq. (14). The velocity field in the boundary layer can now be finally expressed in the form

$$v_r = g'\left[\frac{z}{\sqrt{\nu t}}\right]\frac{r}{t}, \quad v_z = -2g\left[\frac{z}{\sqrt{\nu t}}\right]\frac{\sqrt{\nu}}{\sqrt{t}}, \tag{18}$$

while the expression for the wall shear stress is obtained as

$$\tau_w = 1.0354\sqrt{\nu}\rho r t^{-3/2}. \tag{19}$$

B. Asymptotic behavior of the flow

It is often very convenient to obtain a solution for a flow in an explicit analytical form. Such form can be useful in further analysis related to the considered flows, for example, in the description of heat transfer, phase change, or diffusion. Moreover, since the ordinary differential equation (14) for the scaled stream function g has to satisfy the boundary condition (16) at infinity, it is important to check whether a converging asymptotic solution exists at large ξ.

1. Asymptotic behavior at $\xi \gg 1$

Consider an asymptotic solution of Eq. (14) at large ξ. Assume the scaled stream function $g(\xi)$ in the form

$$g(\xi) = \xi - \gamma + \epsilon(\xi), \tag{20}$$

where $\epsilon(\xi)$ is small if $\xi \gg 1$. Equation (14) can be linearized for small ϵ:

$$\epsilon''' - 2\gamma\epsilon'' + \tfrac{5}{2}\xi\epsilon'' - \epsilon' = 0. \tag{21}$$

A general solution of Eq. (21) is obtained in the following form:

$$\epsilon'(\xi) = \exp\left[2\gamma\xi - \frac{5\xi^2}{4}\right]\left\{H_{-7/5}\left(\frac{-4\gamma+5\xi}{2\sqrt{5}}\right)C_1 + {}_1F_1\left(\frac{7}{10};\frac{1}{2};\frac{(4\gamma-5\xi)^2}{20}\right)C_2\right\}, \tag{22}$$

where $H_n(\cdot)$ is the Hermite polynomial, ${}_1F_1(\cdot)$ is the Kummer confluent hypergeometric function, and C_1 and C_2 are the integration constants. The term corresponding to the coefficient C_2 diverges at $\xi \to \infty$. Therefore C_2 must vanish and the outer approximation of the function g' can thus be reduced using Eqs. (22) and (20) to the following form:

$$g'_{\text{out}}(\xi) = 1 + C_1 \exp\left[2\gamma\xi - \frac{5\xi^2}{4}\right]H_{-7/5}\left(\frac{-4\gamma+5\xi}{2\sqrt{5}}\right). \tag{23}$$

It can be shown that function $g'_{\text{out}}(\xi)$ approaches unity at $\xi \to \infty$ for any finite C_1 which satisfies the boundary condition (16).

Let us try to roughly estimate the constants C_1 and γ from the boundary conditions (15),

$$g'_{\text{out}}(0) = 0, \tag{24}$$

$$\int_0^\infty g'_{\text{out}}(\xi) = -\gamma. \tag{25}$$

Conditions (24) and (25) with the help of Eq. (23) form a system of transcendental equations which can be solved numerically. The roots of this system are $\gamma = 0.626$ and $C_1 = -0.537$. The obtained approximate solution is

$$g'_{\text{out}}(\xi) = 1 - 0.54\exp[1.25\xi - 1.2\xi^2]H_{-7/5}(1.12\xi - 0.56). \tag{26}$$

In Fig. 8 asymptotic solution (26) is compared with the results of numerical calculations of $g'(\xi)$. It is amazing that despite the fact that our approximation should not be valid near the wall, where $\xi \ll 1$, $\epsilon = \mathcal{O}(1)$, and $\epsilon' = \mathcal{O}(1)$, the approximate solution (26) is rather close to the numerical solution on the entire interval of ξ.

Downloaded 04 Oct 2013 to 141.161.91.14. This article is copyrighted as indicated in the abstract. Reuse of AIP content is subject to the terms at: http://pof.aip.org/about/rights_and_permissions

2. Asymptotic behavior at $\xi \ll 1$

Small values of ξ correspond to the near-wall region where the velocities are small ($g \ll 1$, $g' \ll 1$). In this case the terms of order ξ^2 can be neglected. The linearized equation (14) has the following form:

$$g''' + \tfrac{1}{2}\xi g'' + g' = 0. \tag{27}$$

In the derivation of Eq. (27) we have used the assumption $g \ll \xi < 1$. An adequateness of this assumption will be checked *a posteriori*. The solution of Eq. (27) which satisfies the initial conditions $g(0)=0$ and $g'(0)=0$ is

$$g_{\text{in}} = 2g''(0)\left(1 - \exp\left[-\frac{\xi^2}{4}\right]\right), \tag{28}$$

$$g'_{\text{in}} = g''(0)\exp\left[-\frac{\xi^2}{4}\right]. \tag{29}$$

It can be shown that $g_{\text{in}} \approx g''(0)\xi^2/2 \ll \xi$ if $\xi \ll 1$. Therefore the assumed form of Eq. (27) was adequate.

Function g'_{in} has an extreme point at $\xi=\sqrt{2}$ and decays at $\xi \to \infty$. The inner solution is thus not able solely to describe the behavior of the scaled stream function g at large ξ. Therefore the inertial effects associated with the flow velocity are significant even in the boundary layer and cannot be neglected in the analysis of film spreading.

In Fig. 8 the asymptotic solution for the scaled stream function (29) is shown for $g''(0)=1.0354$ obtained from the numerical solution. The solution agrees well with the numerical results on the interval $\xi < 1$.

The integration constants in the outer and inner solutions could be determined from the matching conditions in an intermediate region at values of ξ comparable to unity. However, we do not perform the matching procedure since our numerical solution completely satisfies the purpose of the present study, namely, the description of drop spreading on a dry rigid substrate.

III. RESULTS AND DISCUSSIONS

A. Evolution of the film thickness

At the distances from the substrate significantly exceeding the typical thickness of the boundary layer, $z > \delta$, the scaled stream function $g(\xi)$ approaches its asymptotic value $g(\xi) \to \xi - \gamma$. The corresponding axial velocity in the spreading film outside the boundary layer is therefore

$$v_z = -\frac{2z}{t} + 2\gamma\frac{\sqrt{\nu}}{\sqrt{t}} \quad \text{at} \quad z > \delta. \tag{30}$$

The thickness of the spreading film can be now determined from the ordinary differential equation

$$\dot{h} = -\frac{2h}{t} + 2\gamma\frac{\sqrt{\nu}}{\sqrt{t}} \quad \text{at} \quad h > \delta, \tag{31}$$

the solution of which is

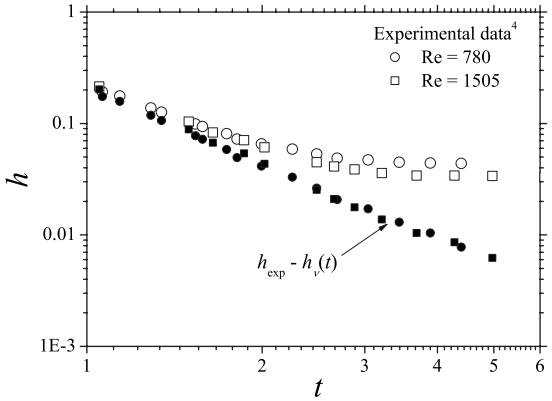

FIG. 9. Drop impact onto a spherical target. Evolution of the film thickness h at the impact axis as a function of time in comparison with the inviscid thickness estimated as $h_{\text{expt}}-h_\nu(t)$. The experimental data for h_{expt} are from Fig. 9 in Ref. 4. The target–to-drop diameters ratio is $D_{\text{target}}=2.7$.

$$h = h_{\text{inv}} + h_\nu(t), \quad h_{\text{inv}} = \frac{\eta}{t^2}, \quad h_\nu = \frac{4\gamma}{5}\frac{\sqrt{t}}{\sqrt{\text{Re}}}. \tag{32}$$

The expression for the film thickness consists of the "inviscid" part, h_{inv}, in the form predicted by the remote asymptotic solution[17] and of the viscous thickness increment $h_\nu(t)$. The viscous thickness increment h_ν is negligibly small at the initial stages of drop spreading if the Reynolds number is very high. However, at long times and small film thicknesses this additional term becomes significant.

In order to discuss the importance of the thickness increment h_ν in the expression for the film thickness [Eq. (32)] we consider experimental data from Ref. 4 on drop impact onto a rigid spherical target. In Fig. 9 the experimental data from Fig. 9 in Ref. 4 for the film thickness h_{expt} at the impact center is compared with the inviscid part $h_{\text{inv}}=h_{\text{expt}}-h_\nu$, where h_ν is defined in Eq. (32). The difference is rather significant at large times. As predicted by the theory, the value of $h_{\text{expt}}-h_\nu$ does not depend on Reynolds number even for the relatively large times after impact. The target-to-drop diameter ratio in these experiments is $D_{\text{target}}=2.7$. It should be noted that during most time of drop spreading, the values of the drop height h_{expt} for both Reynolds numbers are very similar. For the theory, validation is therefore important that the reduction of the film thickness on h_ν even improves this agreement (or at least does not destroy it). The inviscid part $h_{\text{expt}}-h_\nu$ follows closely an inverse square law on time in the form predicted in Ref. 17.

In Fig. 10 the estimated inviscid part of the film thickness, $h_{\text{inv}}=h_{\text{expt}}-h_\nu$, is shown for various Reynolds numbers using the experimental data from Fig. 10 in Ref. 4. The target-to-drop diameter ratio is $D_{\text{target}}=2.3$. The data points lie approximately in one curve at the initial stage of drop spreading and diverge at larger times. There are two possible explanations for this divergence which already have been given in Ref. 4. The first reason is the motion of a rim formed at the edge of the spreading lamella. If the target is partially wettable the rim reaches the maximum radius and then recedes. At some instant the rim starts to merge leading to the quick increase in the film thickness at the impact axis,

Downloaded 04 Oct 2013 to 141.161.91.14. This article is copyrighted as indicated in the abstract. Reuse of AIP content is subject to the terms at: http://pof.aip.org/about/rights_and_permissions

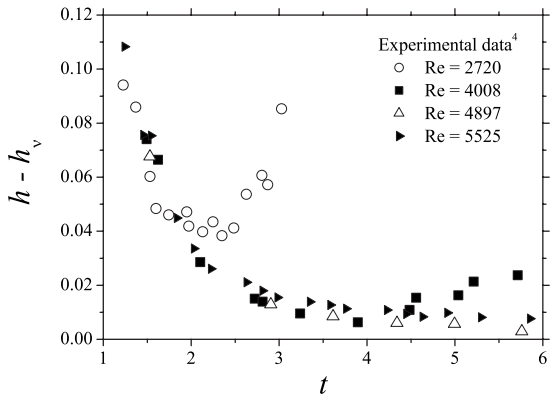

FIG. 10. Drop impact onto a spherical target. Evolution of the inviscid film thickness estimated as $h_{\text{expt}}-h_{\nu}(t)$ for various Reynolds numbers. The experimental data for h_{expt} are from Fig. 10 in Ref. 4. The target-to-drop diameters ratio is $D_{\text{target}}=2.3$.

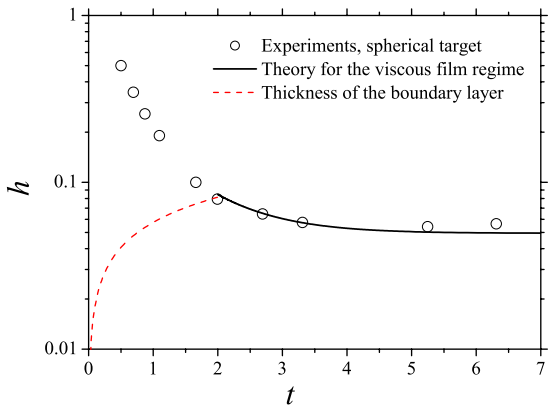

FIG. 11. (Color online) Drop impact onto a spherical target with Re =1068. Experimental data (Ref. 4) on the dimensionless drop height at the target top as a function of the dimensionless time in comparison with the thickness of the boundary layer [Eq. (33)] and with the theoretical predictions (35) for the viscous film regime.

as in the case of Re=2720 in Fig. 10. The second reason is related to the thickness of the boundary layer. When the predicted thickness δ is higher than the lamella thickness the solution derived in Sec. II is not longer valid since it does not satisfy the shear-stress-free condition at the film free boundary. The flow in the lamella is then influenced significantly by the viscosity. This regime is considered in Sec. III B.

B. Film flow governed by viscosity

The thickness of the boundary layer can be expressed using Eq. (17). The dimensionless thickness can therefore be roughly estimated as

$$h_{\text{BL}} = 1.88\sqrt{t/\text{Re}}, \tag{33}$$

where the drop initial diameter is used as the length scale and the impact velocity as the velocity scale. The time t_{BL} at which the boundary layer reaches the free surface of the lamella at the axis can be estimated from the condition $h_{\text{BL}}=h$.

At times $t>t_{\text{BL}}$ the flow in the lamella is governed mainly by the balance between liquid inertia and viscosity. The flow on a spherical substrate in this regime has been estimated in Ref. 4. In the case of a flat substrate this analysis can be simplified. The evolution equation for the approximate film thickness on a planar surface can be obtained in the dimensionless form

$$\ddot{h} - \frac{9}{5}\frac{\dot{h}^2}{h} + \frac{3}{\text{Re}}\frac{\dot{h}}{h^2} = 0, \tag{34}$$

where the first two terms are associated with the inertial effects and the third term is associated with the viscosity.

The solution for the film thickness can be expressed as

$$t = t_{\text{BL}} + \int_h^{h_0} \left[\left(V_0 + \frac{15}{14\text{Re}h_0} \right) \frac{h^{9/5}}{h_0^{9/5}} - \frac{15}{14\text{Re}h} \right]^{-1} dh. \tag{35}$$

At some time instant the velocity in the lamella almost vanishes while the film thickness approaches some asymptotic value determined in Ref. 4. The residual film thickness can be estimated from the solution of Eq. (35),

$$h_{\text{res}} = \frac{h_0^{9/14}}{\left(\frac{1}{h_0} + \frac{14\text{Re}V_0}{15} \right)^{5/14}}. \tag{36}$$

The lamella formed by axisymmetric drop impact onto a rigid spherical target of the dimensionless diameter D_{target} is a more general case of the impact onto a flat target (which corresponds to $D_{\text{target}}\to\infty$). In Fig. 11 the experimental data for the drop height at the axis are shown for the impact parameters Re=1068, We=144 and the target-to-drop diameter ratio $8.8\gg 1$. At small times the thickness of the boundary layer is smaller than the drop height. At the time instant $t\approx 2.0$ it reaches the top of the drop. At times $t>2.0$ the evolution of the film thickness is calculated using the approximate solution (35) with the initial conditions for h_0 and V_0 estimated from the experiments at the time instant $t=t_{\text{BL}}=2.0$. The agreement between the theory and the experimental data is rather good indicating that the time instant t_{BL} is determined precisely.

The similar comparison between the theory and the results of the numerical simulations[13] of drop impact onto a flat

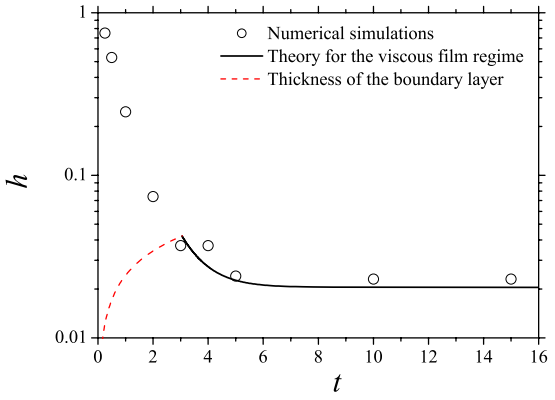

FIG. 12. (Color online) Drop impact onto a flat surface with Re=6020. Numerical simulations (Ref. 13) of the drop height at the axis as a function of time in comparison with the thickness of the boundary layer [Eq. (33)] and with the theoretical predictions (35) for the viscous film regime.

Downloaded 04 Oct 2013 to 141.161.91.14. This article is copyrighted as indicated in the abstract. Reuse of AIP content is subject to the terms at: http://pof.aip.org/about/rights_and_permissions

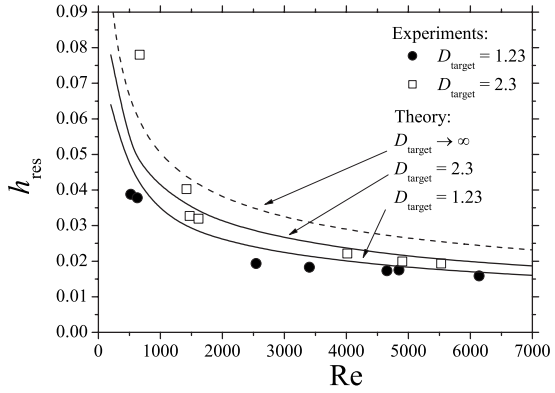

FIG. 13. Drop impact onto a spherical target. Experimental data (Ref. 4) for the dimensionless residual film thickness at the axis as a function of the impact Reynolds number for various dimensionless target diameters in comparison with the theoretical estimations (36). The theoretical data corresponding to a flat substrate, $D_{target} \to \infty$, are obtained using Eq. (39).

rigid substrate with Re=6020, We=117 is shown in Fig. 12. In order to validate the theoretical predictions for the residual film thickness for different Reynolds numbers we use the experimental data[4] for the evolution of the drop height at the impact axis. From these experiments the inviscid part of the dimensionless film thickness $h_{inv}=h_{expt}-h_{\nu}$ can be estimated and then fitted by a more general function,[18]

$$h_{inv} = \frac{\eta}{(t+\tau)^2}. \tag{37}$$

Here τ and η are fitting parameters.

The time instant t_{BL} which is the root of the equation $h_{BL}=h_{inv}(t_{BL})+h_{\nu}(t_{BL})$ can be determined numerically for a given Reynolds number. The rate of the film thinning is then estimated using $V_0=-dh/dt$ at $t=t_{BL}$.

In Fig. 13 the results of the estimations (36) of the residual thickness of the lamella formed by drop impact onto a sphere are compared with the experimental data shown in Fig. 11 in Ref. 4. The values of the constants in Eq. (37) are $\{\eta=0.135,\ \tau=-0.137\}$ for $D_{target}=2.3$ and $\{\eta=0.065,\ \tau=0.32\}$ for $D_{target}=1.23$. The agreement is rather good for most of the impact parameters if the Reynolds number is significantly larger than unity.

There is one case with the Reynolds number Re=665, $D_{target}=2.3$, in which the residual thickness of the lamella drastically increases in comparison to the theoretical predictions (36). The growth of the residual film thickness at relatively "small" Reynolds numbers is caused by the rim receding and merging and the corresponding propagation of the capillary wave. This rim merging is governed by the surface tension and by the force associated with the target wettability.

Let us approximate the evolution of the film thickness in the case of drop impact onto a flat substrate at large times by Eq. (32) and neglect the small constant τ. This rough estimation yields $t_{BL} \approx 0.87\eta^{2/5}\mathrm{Re}^{1/5}$. The thickness of the lamella at the time instant $t=t_{BL}$ and the rate of the thickness thinning at this time instant are obtained in the following form:

$$h_0 \approx 1.76\eta^{1/5}\mathrm{Re}^{-2/5}, \quad V_0 \approx 2.74\eta^{-1/5}\mathrm{Re}^{-3/5}. \tag{38}$$

Finally, the expression for the residual film thickness resulting from the normal impact of a drop onto a smooth flat substrate estimated using $\eta=0.39$ (see Ref. 18) and Eq. (36) can be written in the following simple form:

$$h_{res} = 0.79\mathrm{Re}^{-2/5}, \tag{39}$$

which is valid for very high magnitudes of the impact Reynolds number. This theoretical curve is also shown in Fig. 13.

C. Maximum spreading diameter: Engineering correlation

The maximum spreading diameter D_{max} is one of the important parameters characterizing drop impact. This parameter mainly depends on the impact Weber and Reynolds numbers and on the substrate wettability. If the Weber and Reynolds numbers are high, the effect of wettability is relatively small.[22] It was recently shown[18] that the energy balance approach, frequently used in the development of the models for the maximum spreading diameter, cannot reliably describe the flow in the impacting drop.

A single, universal, and reliable expression for D_{max} cannot be easily formulated as a combination of the Reynolds and Weber numbers since the model based on the physical understanding of the phenomena has to account for several modes of spreading.

The *first mode* corresponds to the relatively small impact parameters, We<10 or Re$<10^2$, when the flow in the entire deforming drop is governed by the viscosity and capillary forces.[18] If both impact parameters are high enough, We$\gg 10$ or Re$\gg 10^2$, the drop shape can be represented as a radially spreading lamella bounded by a rim. The flow in the lamella is inertia dominated; it does not depend on the impact parameters, whereas the rim motion is governed by the surface tension and viscosity. The *second mode* corresponds to the case when the capillary forces are so significant that the rim diameter reaches the maximum at the time instant $t_{max}<t_{BL}$, before the boundary layer reaches the upper free surface of the lamella. The *third mode* corresponds to the case when $t_{max}>t_{BL}$ and the maximum spreading diameter is determined mainly by the viscous effects.

Consider the third mode of spreading when the maximum spreading diameter corresponds to the instant when the flow in the thin lamella is damped by the viscosity. In the limit of infinite Weber number the volume accumulated in the rim can be neglected. The residual film thickness is approximately uniform and the residual drop shape can be roughly approximated by a disk of thickness h_{res}. The maximum drop diameter can be roughly estimated from the mass balance as

$$D_{max\,\infty} \sim \sqrt{\frac{2}{3h_{res}}} = 0.78\mathrm{Re}^{1/5}. \tag{40}$$

The magnitude of $D_{max\,\infty}$ is proportional to $\mathrm{Re}^{1/5}$, as obtained recently in Ref. 6 from energy considerations. On the other hand, the value of the maximum spreading diameter is influenced by the appearance of the rim since the

Downloaded 04 Oct 2013 to 141.161.91.14. This article is copyrighted as indicated in the abstract. Reuse of AIP content is subject to the terms at: http://pof.aip.org/about/rights_and_permissions

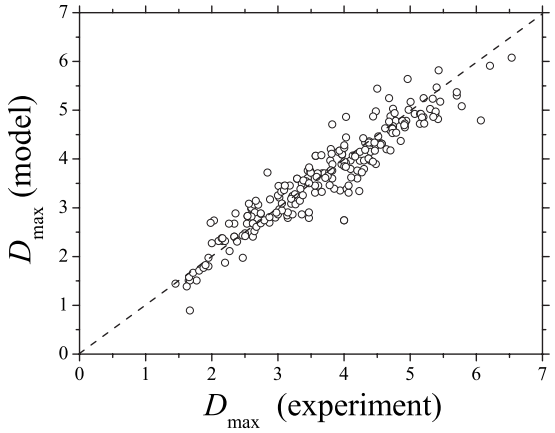

FIG. 14. Single drop impact onto a dry substrate. Comparison of relation (42) for the dimensionless maximum spreading diameter with the experimental data (Refs. 3, 7, 8, and 10).

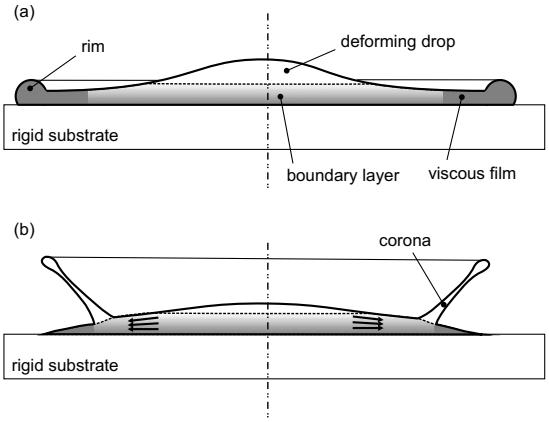

FIG. 15. Sketch of the drop impacting onto a dry substrate with high Reynolds and Weber numbers: drop spreading (a) and film splash (b).

Weber number is finite. The typical length scale L_R associated with the rim motion can be obtained with the help of the rim relative velocity[1] in the following form:

$$L_R \sim t_{\mathrm{BL}}\mathrm{We}^{-1/2}h_{\mathrm{res}}^{-1/2} = 0.61\mathrm{Re}^{2/5}\mathrm{We}^{-1/2}. \quad (41)$$

The maximum drop diameter should decrease if the length scale L_R increases. The wettability properties of a substrate also influence the value of L_R. Nevertheless, accurate experiments[10,22] has shown that the effect of wettability on the value of the maximum spreading diameter is minor if the Reynolds and Weber numbers are high.

We fit the experimental data[3,7,8] for the maximum spreading diameter using the linear combination of the terms defined in Eqs. (40) and (41). The obtained semiempirical relation is

$$D_{\max} \approx 0.87\mathrm{Re}^{1/5} - 0.40\mathrm{Re}^{2/5}\mathrm{We}^{-1/2}. \quad (42)$$

It should be noted that the terms in the right-hand side of Eq. (42) are in the same order of magnitude as the terms determined in Eqs. (40) and (41). The results of comparison between the predictions (42) and the experimental values for the maximum spreading diameter are shown in Fig. 14. The agreement is rather good in the entire range of impact parameters.

The effect of the viscous stresses on the rim velocity is neglected in our scaling analysis since in all the considered experiments the ratio of the viscous force to the surface tension, $\mathrm{We}h_{\mathrm{res}}/\mathrm{Re} \approx \mathrm{WeRe}^{-7/5}$, is negligibly small. For very viscous liquids or very small drops this term can become significant and the proposed simple scaling relation (42) will no longer be valid.

D. Mechanisms of crown formation

If the impact Weber and Reynolds numbers are high enough the radially expanding lamella does not continue to spread on a substrate. At some instant it generates almost axisymmetric uprising sheet.[23] Its shape is very similar to the corona sheet generated by drop impacting onto a uniform stationary film. The mechanism of crown formation produced by drop impact onto a wetted substrate is absolutely clear. It can be explained[17] by propagation of a kinematic discontinuity which divides the inner radially expanding flow initiated by drop impact and the outer undisturbed film. Interaction of these two flows leads to the generation of an upraising sheet.[24]

Various explanations can be found in the literature for the mechanism of corona breakup leading to the generation of secondary drops. Most often breakup occurs at the edge of the crown while in some rare cases the rim simply detaches from the corona and very quickly breaks up due to the Rayleigh capillary instability.[25] The breakup leads to the creation of fingerlike jets almost uniformly distributed along the rim. These jets are almost parallel to the median surface of the free uprising sheet at the edge and always directed ahead the flow in the corona. An extended statistical data for the interjet distances[25] shows that the typical breakup length is related to the rim characteristic diameter and is very similar to the predictions by the Plateau–Rayleigh instability theory. However this theory, which considers axisymmetric disturbances of a free infinite cylindrical jet, is not able to predict the ordered direction of the fingers which are always normal to the rim axis. This conclusion is confirmed also by the numerical simulations of rim propagation.[26] The direction of the fingers and the close relation of the interfinger distance to the rim diameter cannot be explained also by the Richtmyer–Meshkov instability which has been recently proposed as a possible mechanism of splash.[27] On the other hand the transverse rim instability mechanism[28] explains the rim bending and appearance of the jets in the plane of the liquid sheet. The theoretical predictions of the interjet length agree well with the experimental data.[25] Some other effects, for example, the distortion of the rim cross section due to its acceleration[29] and internal viscous stresses, could probably also affect the rim dynamics and even lead to its short-wave breakup.

In the case of drop impact onto a dry wall the outer film region is absent before impact. What is the nature of the force applied to the lamella edge in the normal to substrate direction?

Consider the fast drop spreading and the boundary layer shown schematically in Fig. 15(a). Immediately after impact

Downloaded 04 Oct 2013 to 141.161.91.14. This article is copyrighted as indicated in the abstract. Reuse of AIP content is subject to the terms at: http://pof.aip.org/about/rights_and_permissions

the boundary layer is developed near the substrate. Its thickness increases in time. Since the thickness of the lamella is thinner at the edges than at the center[18] the boundary layer first reaches the upper free surface of the lamella at the edge region. The spreading drop can be now subdivided into three regions: deforming drop above the boundary layer, boundary layer in the central part of the drop, and the stationary film at the outer region of the spreading lamella.

Therefore, even in the case of drop impact onto an initially dry substrate, shortly after drop collision the situation is very similar to drop impact onto a thin stationary film. The fast radially expanding flow in the central part of the deforming drop interacts with the outer stationary liquid layer. If the impact parameters exceed a splashing threshold, such interaction leads to corona formation and splash.

Experiments with water drop impacts onto a dry wall[30] show that the secondary drops resulting from splash move with the velocity approximately twice of the velocity of the crown base (see their Fig. 15). This fact is in confirmation with the theoretical predictions[17] based on the kinematic discontinuity approach.

In order to determine the splashing threshold we follow the logical chain proposed for the description of splashing threshold of the train of drops in Ref. 17. At the kinematic discontinuity the film flow is governed by the inertia and capillary forces. The dimensionless pressure associated with the surface tension is $p_\sigma \sim \mathrm{We}^{-1}\partial^2 h/\partial r^2 \sim \mathrm{We}^{-1}h_{\mathrm{res}}$, whereas the dimensionless pressure term associated with the liquid inertia is comparable to unity. The splash occurs when $p_\sigma \ll 1$. This condition with the help of Eq. (36) yields the following expression for the splashing parameter:

$$S_{\mathrm{film}} = \mathrm{WeRe}^{2/5} \gg 1. \tag{43}$$

Drop impact leads to splash if the parameter S_{film} is higher than the large threshold value S_c.

This expression is very similar to the well known splashing parameter $K=(\mathrm{WeRe}^{1/2})^{4/5}$ obtained by fitting of the experimental data.[31,32] Other experiments[30,33] allow to predict the splashing condition in the form $S_{\mathrm{expt}}=\mathrm{WeRe}^{0.44}>3.45\times10^4$ (in the case of polished stainless steel substrate of roughness $R_a=0.05$ μm). This form is even closer to the theoretically predicted expression (43).

It should be noted that the expression for the splashing parameter [Eq. (43)] is not universal. The splash can be enchased by the surface roughness[34] or reduced by the substrate elasticity.[35] Another factor which can influence the splash is the formation of the rim at the edge of the lamella. If the Weber number is relatively low the outer stationary region of the lamella can be covered by the rim before the onset of splash even if the Reynolds number is extremely high.

In some cases (for example, drop impact of a volatile liquid under reduced pressure conditions) the evaporation of the thin film of thickness h_{res} can influence the value of the splashing threshold. On the other hand such evaporation cannot completely explain[36] the strong dependence of the surrounding pressure on the value of the splashing threshold[37] in the case of impact of low-viscosity, low-surface-tension, volatile liquids.

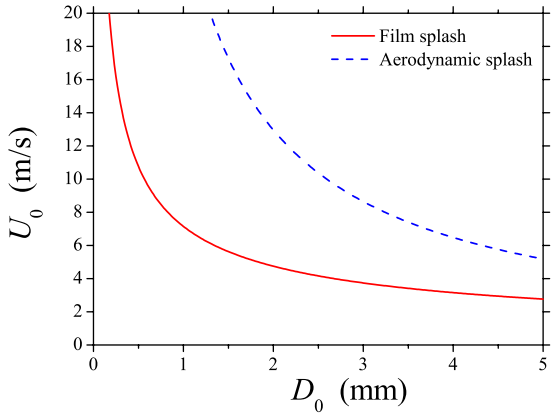

FIG. 16. (Color online) Thresholds for the film splash and aerodynamic splash for water in air at normal conditions.

This is a spectacular and presently rather disputable experimental result. The mechanism of corona formation is explained[37] by the action of the aerodynamic stresses related to the propagation of a weak shock. The splashing parameter is defined by

$$S_{\mathrm{aero}} = \frac{\rho_g}{\rho}\frac{c_g}{U_0}\mathrm{WeRe}^{-1/2} \approx 0.9, \tag{44}$$

where ρ_g is the gas density and c_g is the speed of sound.

Figure 16 shows the comparison of the thresholds for the film splash[30] and for the aerodynamic splash expressed in Eq. (44) for the case of water drop impact ($\rho=10^3$ kg/m^3, $\sigma=7.3\times10^{-2}$ N/m, and $\nu=10^{-6}$ m^2/s) in air at normal conditions ($\rho_g=1.2$ kg/m^3 and $c_g=340$ m/s). In the entire range of drop diameters the film splash threshold is below the aerodynamic threshold. Therefore, water drop impact is characterized exclusively by the film splash expressed in Eq. (43).

The same graphs for the methanol drop are shown in Fig. 17. The results are phenomenologically different. Methanol drops of diameter smaller than one mm splash due to the lamella interaction with the film at rest (film splash) while the drops of diameter larger than 1 mm (the range

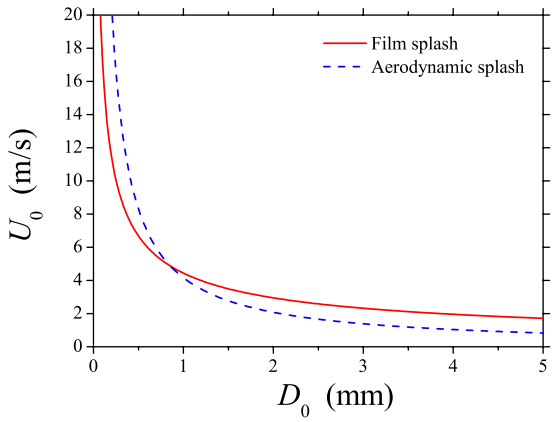

FIG. 17. (Color online) Thresholds for the film splash and aerodynamic splash for methanol in air at normal conditions.

Downloaded 04 Oct 2013 to 141.161.91.14. This article is copyrighted as indicated in the abstract. Reuse of AIP content is subject to the terms at: http://pof.aip.org/about/rights_and_permissions

corresponding to the experiments in Ref. 37) splash due to the aerodynamic effects near the contact line.

These two mechanisms of splash probably do not describe all the possibilities related to drop impact and splash. For example, none of these two models can predict well the splashing threshold parameters in the experiments in Ref. 38. The entire picture of splash still remains undiscovered.

IV. CONCLUSIONS

The present study is devoted to the analysis of the viscous effects associated with the fast drop spreading. A self-similar solution for the viscous flow in the drop is obtained which satisfies the full Navier–Stokes equations. The expression for the thickness of the boundary layer is used for the estimation of the residual film thickness on the substrate. The theoretical predictions are compared with the experimental data on drop impact onto a spherical target. The agreement is rather good.

Next, the assumption on the universal flow in the lamella[18] with the help of the expression for the residual film thickness allows us to develop a new scaling relation for the drop maximum spreading diameter. The semiempirical expression for maximum spreading diameter agrees well with the experimental data from the literature in a wide range of parameters.

Several mechanisms leading to the emergence of a crownlike upraising sheet are considered in this study, aerodynamic splash[37] and film splash. The mechanism of the film splash can be described well by the propagation of the kinematic discontinuity.[17]

[1] G. I. Taylor, "The dynamics of thin sheets of fluid. II. Waves on fluid sheets," Proc. R. Soc. London, Ser. A **253**, 296 (1959).
[2] F. E. C. Culick, "Comments on a ruptured soap film," J. Appl. Phys. **31**, 1128 (1960).
[3] I. V. Roisman, R. Rioboo, and C. Tropea, "Normal impact of a liquid drop on a dry surface: Model for spreading and receding," Proc. R. Soc. London, Ser. A **458**, 1411 (2002).
[4] S. Bakshi, I. V. Roisman, and C. Tropea, "Investigations on the impact of a drop onto a small spherical target," Phys. Fluids **19**, 032102 (2007).
[5] A. L. Yarin, "Drop impact dynamics: Splashing, spreading, receding, bouncing," Annu. Rev. Fluid Mech. **38**, 159 (2006).
[6] C. Clanet, C. Béguin, D. Richard, and D. Quéré, "Maximal deformation of an impacting drop," J. Fluid Mech. **517**, 199 (2004).
[7] M. Pasandideh-Fard, Y. M. Qiao, S. Chandra, and J. Mostaghimi, "Capillary effects during droplet impact on a solid surface," Phys. Fluids **8**, 650 (1996).
[8] L. Cheng, "Dynamic spreading of drops impacting onto a solid surface," Ind. Eng. Chem. Process Des. Dev. **16**, 192 (1977).
[9] H. Marmanis and S. T. Thoroddsen, "Scaling of the fingering pattern of an impacting drop," Phys. Fluids **8**, 1344 (1996).
[10] B. L. Scheller and D. W. Bousfield, "Newtonian drop impact with a solid surface," AIChE J. **41**, 1357 (1995).
[11] E. W. Collings, J. K. Markworth, J. K. McCoy, and J. H. Saunders, "Splat-quench solidification of freely falling liquid-metal drops by impact on a planar substrate," J. Mater. Sci. **25**, 3677 (1990).
[12] S. Chandra and C. T. Avedisian, "On the collision of a droplet with a solid surface," Proc. R. Soc. London, Ser. A **432**, 13 (1991).
[13] J. Fukai, Y. Shiiba, T. Yamamoto, O. Miyatake, D. Poulikakos, C. M. Megaridis, and Z. Zhao, "Wetting effects on the spreading of a liquid droplet colliding with a flat surface: Experiment and modeling," Phys. Fluids **7**, 236 (1995).
[14] I. V. Roisman, "Dynamics of inertia dominated binary drop collisions," Phys. Fluids **16**, 3438 (2004).
[15] C. Ukiwe and D. Y. Kwok, "On the maximum spreading diameter of impacting droplets on well-prepared solid surfaces," Langmuir **21**, 666 (2005).
[16] Š. Šikalo, H.-D. Wilhelm, I. V. Roisman, S. Jakirlic, and C. Tropea, "Dynamic contact angle of spreading droplets: Experiments and simulations," Phys. Fluids **17**, 062103 (2005).
[17] A. L. Yarin and D. A. Weiss, "Impact of drops on solid surfaces: Self-similar capillary waves, and splashing as a new type of kinematic discontinuity," J. Fluid Mech. **283**, 141 (1995).
[18] I. V. Roisman, E. Beberović, and C. Tropea, "Inertia dominated drop collisions. I. On the universal shape of the lamella," Phys. Fluids **21**, 052103 (2009).
[19] K.-L. Pan and I. V. Roisman, "Note on 'Dynamics of inertia dominated binary drop collisions' [Phys. Fluids **16**, 3438 (2004)]," Phys. Fluids **21**, 022101 (2009).
[20] A. L. Yarin, *Free Liquid Jets and Films: Hydrodynamics and Rheology* (Longman & Wiley, Harlow, 1993).
[21] S. Mukherjee and J. Abraham, "Investigations of drop impact on dry walls with a lattice-Boltzmann model," J. Colloid Interface Sci. **312**, 341 (2007).
[22] R. Rioboo, M. Marengo, and C. Tropea, "Time evolution of liquid drop impact onto solid, dry surfaces," Exp. Fluids **33**, 112 (2002).
[23] R. Rioboo, M. Marengo, and C. Tropea, "Outcomes from a drop impact on solid surfaces," Atomization Sprays **11**, 155 (2001).
[24] I. V. Roisman and C. Tropea, "Impact of a drop onto a wetted wall: description of crown formation and propagation," J. Fluid Mech. **472**, 373 (2002).
[25] I. V. Roisman, T. Gambaryan-Roisman, O. Kyriopoulos, P. Stephan, and C. Tropea, "Breakup and atomization of a stretching crown," Phys. Rev. E **76**, 026302 (2007).
[26] J. M. Fullana and S. Zaleski, "Stability of a growing end rim in a liquid sheet of uniform thickness," Phys. Fluids **11**, 952 (1999).
[27] R. Krechetnikov and G. M. Homsy, "Crown-forming instability phenomena in the drop splash problem," J. Colloid Interface Sci. **331**, 555 (2009).
[28] I. V. Roisman, K. Horvat, and C. Tropea, "Spray impact: Rim transverse instability initiating fingering and splash, and description of a secondary spray," Phys. Fluids **18**, 102104 (2006).
[29] J. Eggers, private communication (2007).
[30] C. Stow and M. G. Hadfield, "An experimental investigation of fluid flow resulting from the impact of a water drop with an unyielding dry surface," Proc. R. Soc. London, Ser. A **373**, 419 (1981).
[31] C. Mundo, M. Sommerfeld, and C. Tropea, "On the modelling of liquid sprays impinging on surfaces," Atomization Sprays **8**, 625 (1998).
[32] G. E. Cossali, A. Coghe, and M. Marengo, "The impact of a single drop on a wetted surface," Exp. Fluids **22**, 463 (1997).
[33] W. Samenfink, "Grundlegende Untersuchung zur Tropfeninteraktion mit schubspannungsgetriebenen Wandfilmen," Ph.D. thesis, Universität Karlsruhe, 1997.
[34] K. Range and F. Feuillebois, "Influence of surface roughness on liquid drop impact," J. Colloid Interface Sci. **203**, 16 (1998).
[35] R. E. Pepper, L. Courbin, and H. A. Stone, "Splashing on elastic membranes: The importance of early-time dynamics," Phys. Fluids **20**, 082103 (2008).
[36] L. Xu, W. W. Zhang, and S. R. Nagel, "Xu, Zhang, and Nagel reply," Phys. Rev. Lett. **96**, 179402 (2006).
[37] L. Xu, W. W. Zhang, and S. R. Nagel, "Drop splashing on a dry smooth surface," Phys. Rev. Lett. **94**, 184505 (2005).
[38] R. L. Vander Wal, G. M. Berger, and S. D. Mozes, "The splash/non-splash boundary upon a dry surface and thin fluid film," Exp. Fluids **40**, 53 (2006).

Downloaded 04 Oct 2013 to 141.161.91.14. This article is copyrighted as indicated in the abstract. Reuse of AIP content is subject to the terms at: http://pof.aip.org/about/rights_and_permissions